Journal of
Materials Chemistry A

ROYAL SOCIETY
OF CHEMISTRY

PAPER

View Article Online
View Journal | View Issue

Atomically resolved surface phases of $La_{0.8}Sr_{0.2}MnO_3(110)$ thin films

Cite this: doi:10.1039/d0ta07032g

Received 18th July 2020
Accepted 31st August 2020

DOI: 10.1039/d0ta07032g

rsc.li/materials-a

Giada Franceschi, Michael Schmid, Ulrike Diebold, and Michele Riva *

Electronic Supplementary Information (ESI)

S1. Enlarged atomic-scale STM images

Fig. S1 shows enlarged versions of the atomic-scale STM images of Fig. 2 of the main text for better visibility of the details.

S2. Mn doses in monolayers (ML)

This Section addresses how the horizontal axes of Fig. 2 and Fig. 5(b and c) of the main text, *i.e.*, the relative compositions of the surface structures in terms of Mn cations, have been established. In a nutshell, we have (i) evaluated the number of laser pulses shot on the MnO target required for the transition between adjacent reconstructions, accounting for sticking/re-evaporation effects that affect the effective amount of material deposited; (ii) evaluated the growth rate of Mn atoms in monolayers [ML, where 1 ML is the number of Mn sites — or, equivalently, A sites — in an $(AMnO)_2$ plane of LSMO(110), *i.e.*, 4.64×10^{14} cm^{-2}] by means of a specially designed QCM;[1] (iii) translated the effective number of pulses shot on the MnO target (i) into monolayers of Mn, by using the growth rate from (ii).

Evaluating the number of laser pulses needed to switch between reconstructions

During the first step, *i.e.*, the evaluation of the number of laser pulses needed to switch between adjacent reconstructions, pronounced differences in surface sticking/re-evaporation of the deposited species were observed among the different surface phases, which must be taken into account to determine the effective amount of material needed to switch between the reconstructions. Fig. S2(a) shows the Mn 2p/La 4d XPS intensity ratios corresponding to well-defined LSMO(110) surfaces that were produced by depositing incremental amounts of Mn at 0.2 mbar O_2 at room temperature (RT) followed by O_2 annealing at 700 °C, starting from the (1 × 1) surface of Fig. 2(a) and Fig. S1(a). The intensity ratios are plotted as a function of the number of laser pulses shot on the MnO target. The intensities increase linearly for small amounts deposited, in agreement with the expected enrichment in Mn of the surface, but above a critical Mn enrichment (dashed line) their slope with the deposited pulses decreases drastically. The critical point corresponds to a surface with a structure between those shown in Figs. 3(b) and 3(c), *i.e.*, slightly Mn richer than the fishbone reconstruction. Correspondingly, after overcoming this critical composition, a larger number of pulses is required to detect appreciable changes in the surface structure in STM. XPS measurements reveal that the observed change in slope is obtained after the post-annealing step: Right after RT deposition, the Mn/La signal increases linearly, as expected (not shown); the signal then decreases after annealing at 0.2 mbar O_2 and 700 °C for 1 h.

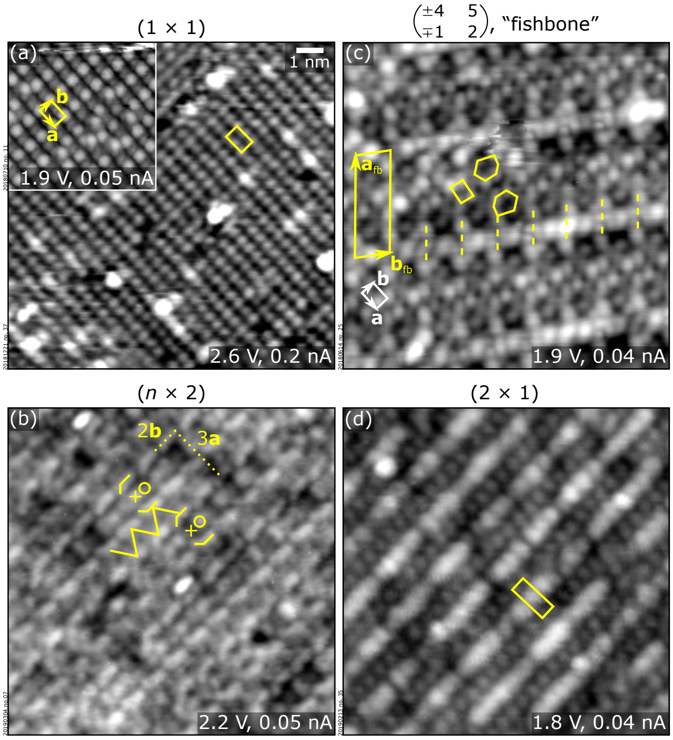

Fig. S1 Enlarged atomic-scale STM images of LSMO(110) (for more information, refer to the phase diagram of Fig. 2 in the main text).

Institute of Applied Physics, TU Wien, Wiedner Hauptstraße 8-10/E134, 1040 Wien, Austria. E-mail: riva@iap.tuwien.ac.at

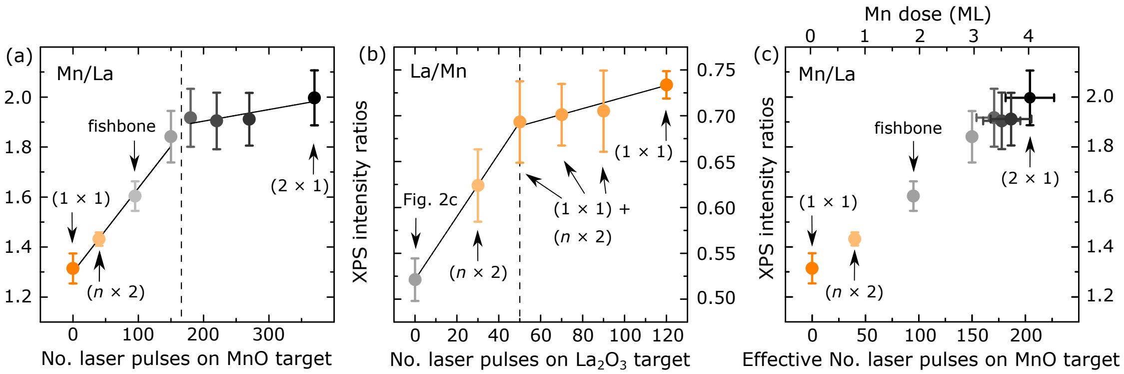

Fig. S2 Surface-dependent re-evaporation of Mn and La species and Mn dose calibration. (a) Mn 2p/La 4d and (b) La 4d/Mn 2p XPS peak intensity ratios as a function of the number of laser pulses shot on the MnO and La_2O_3 targets, to enrich well-defined LSMO(110) surfaces in Mn and La, respectively. (Deposition at RT and 0.2 mbar O_2 plus anneal 1 h, 0.2 mbar O_2, 700 °C.) The XPS intensities are not linear with the number of pulses shot on the targets: Mn (La) species are incorporated less on Mn- (La-)rich surfaces. (c) Mn 2p/La 4d intensity ratios as a function of the "effective" number of laser pulses shot on the MnO target, derived from the data in panel (a) by correcting for the slope differences in the two regimes. The horizontal error bars on the last four points in (c) are due to this correction.

A similar behavior is observed also during the deposition of La. Fig. S2(b) shows the La 4d/Mn 2p XPS intensity ratios as a function of the number of laser pulses shot on the La_2O_3 target (again, deposition at RT in 0.2 mbar O_2, and 700 °C post-annealing in 0.2 mbar O_2). For this set of experiments, the starting point was the Mn-rich structure of Fig. 3(c). The surface becomes increasingly La richer the more La is deposited. As in the case of Mn deposition, the initially linear trend suddenly changes slope after a critical stoichiometry is reached (dashed line). This corresponds to a surface structure between the $(n \times 2)$ and the (1×1).

The data in Fig. S2(a, b) show that, on well-defined LSMO(110) surfaces, Mn (La) species tend to be incorporated less easily in surfaces that are richer in Mn (La), as if there was a large barrier to incorporate additional cationic species when the composition of the surface is brought towards the extremes of the surface phase diagram. Similar trends have been observed previously on $SrTiO_3(110)$, where it was shown they occur because of surface-dependent sticking.[2] One can exclude that the changes in the XPS slopes are associated with the formation of 3D structures, as judged from large-area STM images (not shown). One can also rule out that the change of slope is due to the development of a second layer, as this occurs at Mn doses well above 1 ML. The XPS data acquired right after RT deposition and after post-annealing again suggest that cation re-evaporation upon annealing at 700 °C is the dominant mechanism driving this effect.

The "effective" number of pulses needed to switch between adjacent reconstructions (accounting for the re-evaporated material during the annealing step) has been derived by scaling the number of laser pulses with the slopes of the XPS intensity ratios (obtained from linear fits to the data). The outcome is shown in Fig. S2(c), which displays the structures and Mn/La ratios as a function of the effective number of laser pulses shot on the MnO target (bottom axis) and in terms of monolayers of Mn (top).

Deriving the growth rate of Mn

The translation to monolayers of Mn has been performed by using the amount of Mn deposited per pulse derived with a QCM mounted on a home-designed holder suited for transferring the QCM across the vacuum system.[1] Controlled amounts of material were incrementally deposited on the QCM at the same conditions used for deposition on the LSMO surface (*i.e.*, RT, 0.2 mbar O_2, 1.8 J cm^{-2}), and thereafter the corresponding frequency shifts of the QCM were measured in an adjacent UHV chamber at room temperature (see Fig. S3). From a linear fit of the data in Fig. S3, one derives a rate of change of the resonance frequency of -0.1062 ± 0.0007 Hz per pulse. This corresponds to a mass growth rate $\Delta m/A = 1.32 \pm 0.02$ ng cm^{-2} per pulse.[1]

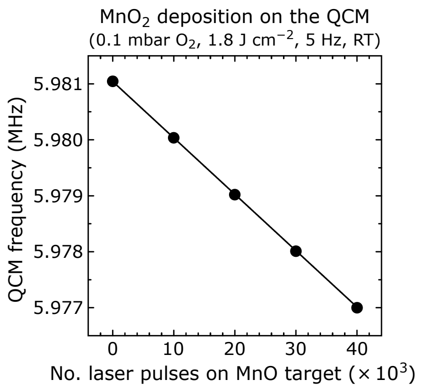

Fig. S3 Shift of the QCM resonance frequency as a function of the amount of MnO_2 deposited (number of laser pulses shot on the MnO target).

Since manganese oxide can exhibit a variety of oxygen stoichiometries (MnO, Mn_2O_3, Mn_3O_4, or MnO_2) depending on the growth conditions, the composition of the films grown on the movable QCM at our conditions was determined by XPS. As shown below, the composition is MnO_2. By accounting for the 1 : 2 Mn : O stoichiometry and the known atomic masses of O and Mn, one can then derive a deposition rate of Mn of $(9.16 \pm 0.15) \times 10^{12}$ Mn at. cm^{-2} per pulse, or $(1.97 \pm 0.03) \times 10^{-2}$ ML of Mn per pulse, where 1 ML is defined as the number of Mn sites in an $(AMnO)_2$ plane of LSMO(110), *i.e.*, 4.64×10^{14} cm^{-2}.

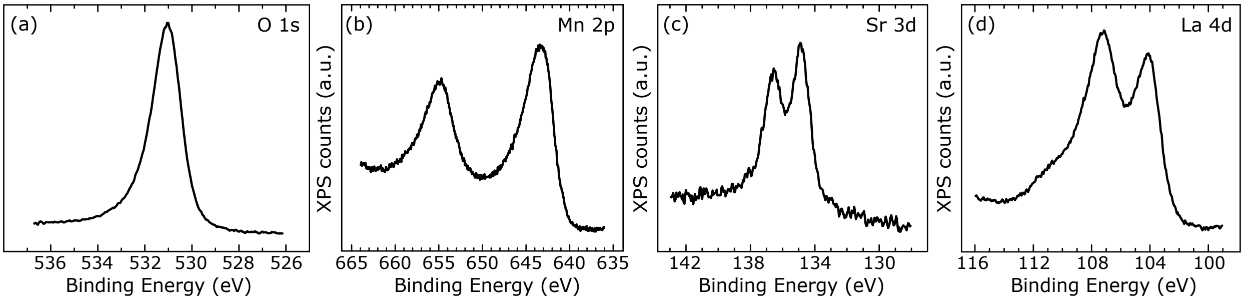

Fig. S4 XPS spectra acquired on a fishbone-reconstructed surface of LSMO(110) (non-monochromatic Al Kα source, normal emission, 10 eV pass energy). The shape of these peaks on the other reconstructions appears identical upon appropriate rescaling.

Table S1 Selected XPS data for different manganese oxides. The Mn 3s splitting, binding energy differences between Mn $2p_{3/2}$ and O 1s, and Mn($2p_{3/2}$, $L_3M_{23}M_{45}$) Auger parameters of several manganese oxide compounds extracted from the literature are compared with values from films grown at room temperature in 0.2 mbar O_2 in the present work on the QCM (rightmost column). Values are expressed in electronvolts. Part of the values are taken from the NIST XPS database;[3] for these, the original references are reported.

	MnO	Mn_3O_4	Mn_2O_3	MnO_2	This exp. (QCM)
Mn 3s splitting			5.4[4]	4.4[5]	4.55 ± 0.22
				4.6[6]	
				4.7[7]	
	5.8[8]	5.3[8]	5.2[8]	4.7[8]	
	6.1[9]		5.5[9]	4.5[9]	
	5.9[10]	4.6[10]	5.2[10]	4.5[10]	
	5.6[11]	5.6[11]	5.4[11]	4.5[11]	
	6.1[12]	5.3[12]	5.4[12]	4.5[12]	
	6.05[13]		5.5[13]	4.58[13]	
$E_b(\mathrm{Mn}\,2p_{3/2}) - E_b(\mathrm{O}\,1s)$			111.8[4]	112.8[5]	112.25 ± 0.05
				112.5[6]	
		111.8[8]	111.8[8]	112.6[8]	
	110.9[11]	111.1[11]	111.4[11]	112.4[11]	
		111.34[14]	111.93[14]	112.36[14]	
		111.6[15]		112.2[15]	
Auger parameter Mn($2p_{3/2}$, $L_3M_{23}M_{45}$)			1226.91[4]	1227.21[5]	1227.24 ± 0.08
				1228.1[6]	
	1223.8[11]	1224.4[11]	1224.6[11]	1225.5[11]	
	1225.6[15]	1224.8[15]	1226.6[15]	1227.3[15]	

Establishing the composition of the manganese oxide film deposited on the QCM

The abundant XPS literature on manganese oxides[4–15] was used to determine the composition of the manganese oxide film deposited on the QCM at our growth conditions. This shows that the shape and the relative positions of few relevant peaks are uniquely associated to a specific compound. MnO is most easily distinguishable, since it displays a characteristic shake-up peak in its Mn 2p spectrum.[12,14] Since this satellite is not present in our spectra (not shown), one can exclude MnO as the dominant composition of the film. Distinguishing between Mn_2O_3, Mn_3O_4, and MnO_2 based on the shape of their peaks is less straightforward, as it hinges on a very accurate fitting of the data, ideally acquired with a monochromatic source.[14] For this reason, the difference of binding energies of Mn $2p_{3/2}$ and O 1s, the final-state splitting of Mn 3s, and the Mn($2p_{3/2}$, $L_3M_{23}M_{45}$) Auger parameter[11] were chosen as indicators. Table S1 summarizes the values extracted from several literature sources. Comparison with our XPS data (rightmost column in Table S1) suggests that the composition of the film deposited on the QCM is largely MnO_2.

S3. XPS spectra

Fig. S4 shows representative XPS spectra for the main core-level peaks of the LSMO(110) surfaces. The spectra in Fig. S4 were measured on a fishbone-reconstructed surface [Fig. 2(c) of the main text and Fig. S2(c)].

References

1 G. Franceschi, M. Schmid, U. Diebold and M. Riva, Movable holder for a quartz crystal microbalance for exact growth rates in pulsed laser deposition, *Rev. Sci. Instrum.*, 2020, **91**, 065003.

2 M. Riva, G. Franceschi, M. Schmid and U. Diebold, Epitaxial growth of complex oxide films: Role of surface reconstructions, *Phys. Rev. Res.*, 2019, **1**, 033059.

3 NIST, *X-ray Photoelectron Spectroscopy Database*, NIST Standard Reference Database Number 20, Version 4.1, National Institute of Standards and Technology, Gaithersburg MD, 20899, U. S. A., 2000, doi:10.18434/t4t88k.

4 M. A. Stranick, Mn_2O_3 by XPS, *Surf. Sci. Spectra*, 1999, **6**, 39.

5 M. A. Stranick, MnO_2 by XPS, *Surf. Sci. Spectra*, 1999, **6**, 31.

6 M. C. Militello and S. W. Gaarenstroom, Manganese dioxide (MnO_2) by XPS, *Surf. Sci. Spectra*, 2001, **8**, 200.

7 J. J. Rosso and M. F. Hochella, Jr., Natural iron and manganese oxide samples by XPS, *Surf. Sci. Spectra*, 1996, **4**, 253.

8 M. Oku and K. Hirokawa, X-ray photoelectron spectroscopy of Co_3O_4, Fe_3O_4, Mn_3O_4, and related compounds, *J. Electron Spectrosc. Relat. Phenom.*, 1976, **8**, 475.

9 J. S. Foord, R. B. Jackman and G. C. Allen, An X-ray photoelectron spectroscopic investigation of the oxidation of manganese, *Philos. Mag. A*, 1984, **49**, 657.

10 L. Z. Zhao and V. Young, XPS studies of carbon supported films formed by the resistive deposition of manganese, *J. Electron Spectrosc. Relat. Phenom.*, 1984, **34**, 45.

11 A. J. Nelson, J. G. Reynolds and J. W. Roos, Core-level satellites and outer core-level multiplet splitting in Mn model compounds, *J. Vac. Sci. Technol. A*, 2000, **18**, 1072.

12 V. Di Castro and G. Polzonetti, XPS study of MnO oxidation, *J. Electron Spectrosc. Relat. Phenom.*, 1989, **48**, 117.

13 G. K. Wertheim, S. Hüfner and H. J. Guggenheim, Systematics of core-electron exchange splitting in 3d-group transition-metal compounds, *Phys. Rev. B*, 1973, **7**, 556.

14 M. C. Biesinger, B. P. Payne, A. P. Grosvenor, L. W. M. Lau, A. R. Gerson and R. S. C. Smart, Resolving surface chemical states in XPS analysis of first row transition metals, oxides and hydroxides: Cr, Mn, Fe, Co and Ni, *Appl. Surf. Sci.*, 2011, **257**, 2717.

15 B. R. Strohmeier and D. M. Hercules, Surface spectroscopic characterization of manganese/aluminum oxide catalysts, *J. Phys. Chem.*, 1984, **88**, 4922.